The potential use of Earth Observing System data to monitor the passive emission of sulfur dioxide from volcanoes

V. J. Realmuto

Jet Propulsion Laboratory, California Institute of Technology
M.S. 168-514
4800 Oak Grove Drive
Pasadena, CA 91109
818-354-1824 (voice)
818-393-6962 (fax)
vince.realmuto@jpl.nasa.gov

Version 2

October 7, 1999

Abstract

Long-term monitoring of the passive emission of SO_2 is essential if volcanologists are to establish baseline emission rates and correlate changes in emission rates with the behavior of a volcano. The synoptic perspective, rapid mode of data acquisition, and short revisit intervals of satellite-based remote sensing are well-suited for the monitoring of SO_2 emissions. This paper evaluates the potential of detecting passive SO_2 emissions from space using the data anticipated from the advanced spaceborne thermal emission and reflection radiometer (ASTER) and moderate resolution imaging spectroradiometer (MODIS). ASTER and MODIS are two of the instruments aboard the first satellite of NASA's Earth Observing System, which is scheduled for a launch in 1999. Image data acquired with NASA's airborne thermal infrared multispectral Scanner (TIMS) over Kilauea and Mount Etna volcanoes were used to simulate the ASTER and MODIS data products. These simulations suggest that both ASTER and MODIS will detect Etna-scale plumes, while reliable detection of Kilauea-scale plumes may be limited to ASTER. In addition, both instruments should be able to detect stratospheric SO_2 clouds of a size and concentration similar to those created by the August 1992 eruption of Mount Spurr.

Introduction

The use of correlation spectroscopy (COSPEC) [*Newcomb and Millán,* 1970; *Moffat and Millán*, 1971] to document SO_2 emission rates is perhaps the most common application of remote sensing to volcanology. Measurements of SO_2 emission rates have yielded a wealth of information regarding magma supply rates [e.g., *Casadevall et al.,* 1981, 1983; *Chartier et al.,* 1988; *Williams et al.,* 1990; *Andres et al.*, 1991], contributions of volcanoes to the global SO_2

budget [e.g., *Stoiber et al.,* 1987; *Berresheim and Jaeschke,* 1993; *Kyle et al.,* 1994; *Graf et al.,* 1997], and emission rates of other constituents of volcanic plumes [e.g., *Rose et al.,* 1986, 1988; *Kyle et al.,* 1990; *Zreda-Gostynska and Kyle,* 1993].

Long-term monitoring of SO_2 emissions have enabled volcanologists to establish baseline emission rates, recognize patterns in the departures from baseline emission, and correlate such patterns with volcanic phenomena [e.g., *Casadevall et al.,* 1983, 1987; *Chartier et al.,* 1988; *McGee,* 1992; *Elias et al.,* 1993, *Caltabiano et al.,* 1994, *Kyle et al.,* 1994; *McGee and Sutton,* 1994; *Daag et al.,* 1996; *Zapata et al.,* 1997]. For example, some eruptions of Mount Etna have been preceded by drops in emission to levels 5 times lower than the baseline rate [*Caltabiano et al.,* 1994]. The 1980 – 1988 record of Mount St. Helens emission rates indicates that exogenous dome-building events were typically preceded by increases in gas emissions [*McGee and Sutton,* 1994], and that emission rates during exogenous dome-building events were 2 to 4 times higher than the rates measured between events [*Casadevall et al.,* 1983]. The wide fluctuations in emission rates prior to the 1991 eruptions of Mount Pinatubo are attributed to a rise of fresh magma followed by a partial sealing of the magma system, the emergence and growth of a lava dome, and a re-opening of the magma system two days before the initial plinian eruption [*Daag et al.,* 1996].

The establishment of a long-term emission-monitoring program can involve considerable labor, expense, logistical planning, and risk to personnel and equipment. Satellite-based remote sensing, which offers synoptic viewing, rapid data acquisition, and repetitive observation, might enable volcanologists to obtain frequent estimates of SO_2 emission at a greater number of volcanoes in a safe and cost-effective manner.

The ability to map the SO_2 content of volcanic plumes and clouds from space was first demonstrated by *Krueger* [1983], using data acquired by the Total Ozone Mapping Spectrometer (TOMS) [*Krueger et al.,* 1995]. TOMS data have been used to track stratospheric SO_2 clouds [e.g., *Krueger,* 1983; *Krueger* et al., 1990; *Doiron et al.,* 1991; *Bluth et al.,* 1992, 1994, 1995], and estimate the contribution of explosive volcanism to the global atmospheric sulfur budget [*Bluth et al.,* 1993, 1997; *Graf et al.,* 1997; *Pyle et al.,* 1996]. However, the coarse spatial resolution of TOMS (50 km at nadir for Nimbus TOMS) has largely precluded the detection of passive SO_2 emission in the troposphere [e.g., *Casadevall et al.,* 1984; *Walter et al.,* 1993].

Two instruments scheduled for a 1999 launch aboard the first satellite of NASA's Earth Observing System will provide image data with higher spatial resolution than TOMS. The advanced spaceborne emission and reflection radiometer (ASTER) and moderate resolution imaging spectroradiometer (MODIS) will produce multispectral thermal infrared (TIR) imagery with spatial resolutions of 90 m and 1 km, respectively, at nadir. *Realmuto et al.* [1994, 1997] have demonstrated that TIR image data acquired by NASA's airborne thermal infrared multispectral scanner (TIMS) could be used to map SO_2 plumes. In this paper TIMS data from Kilauea Volcano (Hawaii) and Mount Etna (Sicily) are used to simulate the data products anticipated from ASTER and MODIS. The simulated data products will be used to determine if the spatial and signal resolution of ASTER and MODIS will be sufficient to detect passive SO_2 emissions on the scale of the Kilauea and Etna plumes.

SO_2 Retrievals in the Thermal Infrared

TIMS, ASTER, and MODIS measure radiance in the 8 – 12 μm atmospheric window, a region of the spectrum where the atmosphere is relatively transparent to TIR radiation. As shown in Figure 1, the presence of SO_2 in the atmosphere reduces atmospheric transmission between 8 and 9.5 μm, with the minimum transmission near 8.5 μm. The TIR SO_2 retrieval algorithm is based on the detection and modeling of this broad absorption feature. However, atmospheric transmission is only one component of the radiance perceived by a spaceborne sensor.

For a vertical path through the atmosphere, the sensor-perceived radiance, L_s, can be described as

$$L_s(\lambda, T_o) = \{\varepsilon(\lambda)B(\lambda, T_o) + [1 - \varepsilon(\lambda)]L_d(\lambda)\}\tau(\lambda) + L_u(\lambda), \quad (1)$$

where T_o represents the ground temperature, $\varepsilon(\lambda)$ represents the ground emissivity, $B(\lambda, T_o)$ represents the Planck function, $\tau(\lambda)$ represents the spectral transmittance of the atmosphere, and $L_u(\lambda)$ and $L_d(\lambda)$ represent the upwelling (or path) and downwelling (or sky) radiance produced by the atmosphere. Sensor-perceived radiance is composed of the ground radiance, $\varepsilon(\lambda)B(\lambda, T_o)$, the fraction of sky radiance reflected from the ground, $[1 - \varepsilon(\lambda)]L_d(\lambda)$, and the path radiance. Atmospheric transmission attenuates the ground radiance and reflected sky radiance are attenuated by atmospheric transmission en route to the sensor. The goal of SO_2 retrieval is to separate the contributions of SO_2 to the perceived radiance from the contributions of the factors discussed above.

When modeling the transfer of radiation through the atmosphere, a common practice is to assume that the atmosphere is composed of parallel, horizontal, and isothermal layers (plane-parallel atmosphere model, cf. *Stephens* [1994]). Each layer acts as a source (emitter) or sink (absorber) of radiation, with the relative strengths of emission and absorption controlled by the

temperature contrast between adjacent layers. In the troposphere, the region of the atmosphere between sea level and approximately 15 km, temperature decreases with increasing altitude. In the stratosphere, the region of the atmosphere between 15 and 50 km, temperature increases with increasing altitude. The terms, $L_u(\lambda)$, $L_d(\lambda)$, and $\tau(\lambda)$ of equation (1) represent the integration of emission and absorption from all of the layers in the model atmosphere.

Non-explosive SO_2 plumes are typically passive, or non-buoyant, due to thermodynamic equilibrium with the surrounding atmosphere. The contrast in the temperatures of the plume and underlying background dictates whether the plume is a net emitter or absorber when observed from space. Emission dominates if the plume is warmer than the background and absorption dominates if the plume is colder than the background.

The TIR SO_2 retrieval is based on the MODTRAN radiative transfer code [*Berk et al.*, 1989], which is used to model the radiance spectrum perceived by a sensor viewing the ground through an intervening SO_2 plume. MODTRAN calculates this radiance using models of the absorption bands of twelve gas molecules (H_2O, CO_2, O_3, N_2O, CO, CH_4, O_2, NO, SO_2, NO_2, NH_3, and HNO_3) together with profiles of atmospheric pressure, temperature, and relative humidity, and the temperature and emissivity of the ground. The SO_2 plume occupies one layer of the model atmosphere.

The retrieval of SO_2 abundance is an underdetermined inverse problem, since none of the aforementioned physical parameters are uniquely determined by the observed radiance spectrum. To create a more tractable inverse problem, information regarding the plume geometry (altitude and thickness) and the surrounding atmosphere are obtained from ancillary sources. The net effect of this additional information is to reduce the inverse problem to a pair of model

parameters: ground temperature and SO_2 concentration. An accurate SO_2 retrieval requires that the radiance be a unique function of ground temperature and SO_2 concentration.

Figure 2 depicts a misfit surface generated with synthetic radiance data. The surface shows the least squares misfit between an "observed" radiance spectrum, calculated with a ground temperature of 305 K and SO_2 concentration of 10 mg m^{-3}, and radiance spectra calculated for ranges of temperatures and concentrations that are centered on the "true" values. Profiles across the misfit surface in the temperature and concentration dimensions (Figure 2) indicate that the surface has a single minimum.

This exercise suggests that unique estimates of temperature and SO_2 concentration can be retrieved from radiance spectra. The gradients of the misfit surface in the temperature and concentration dimensions (Figure 2) show that the ground temperature estimates are much better constrained by the radiance data than the SO_2 concentration estimates. This difference in the determinacy of the model parameters indicates the retrieval process can be simplified by estimating the ground temperature and SO_2 concentration in separate steps.

The transparency of an SO_2 plume at wavelengths longer than 9.5 μm (cf. Figure 1) permits an estimation of the temperature of the ground beneath the plume. The emissivity spectra used to estimate ground temperature and SO_2 concentration are derived from radiance spectra measured from exposures of surface materials that are not obscured by the plume.

The current retrieval procedure requires six runs of MODTRAN. The first spectrum, calculated for a SO_2 concentration of zero, is used to estimate ground temperature. The next five runs use the ground temperature to calculate radiance spectra for an incremental series of SO_2 concentrations. The relationship between perceived radiance and SO_2 concentration defined by

the six radiance spectra is then approximated by a piecewise linear function. Finally, this function is used to find the SO_2 concentration that yields the best least-squares fit to the observed radiance spectrum.

The inputs to the retrieval procedure are the observed radiance spectra, plume geometry (altitude and thickness), ground elevation, and the profiles of atmospheric pressure, temperature and relative humidity. The spectral response of the sensor (cf. Figure 1) is required to resample the MODTRAN output to the resolution of the observed spectra.

The outputs from the retrieval procedure are the ground temperature and SO_2 column abundance (the product of SO_2 concentration and plume thickness) estimates and the final misfit between the observed and model radiance spectra. The ground temperature and misfit are indicators of the accuracy of the retrieval process.

Simulated ASTER and MODIS Data Products

The retrieval of SO_2 and ground temperature estimates from TIMS images of the Mount Etna and Kilauea plumes was discussed in *Realmuto et al.* [1994, 1997], respectively. The following section describes the predicted response of ASTER and MODIS to the presence of Kilauea- and Etna-scale SO_2 plumes. TIMS data, resampled to the spatial resolution of ASTER and MODIS, were used to predict the response of the spaceborne instruments.

Table 1 summarizes the specifications of ASTER [*Kahle et al.*, 1991; *Yamaguchi et al.*, 1998] and MODIS [*Barnes et al.*, 1998]. Both instruments have the requisite spectral channels covering the SO_2 feature at 8.5 μm together with channels at wavelengths longer than 9.5 μm. The main differences between airborne and spaceborne detection of SO_2 emissions are (1) a

decrease in spatial resolution, which reduces, or dilutes, the column abundance estimates by increasing the area covered by an image pixel, and (2) a longer path through the atmosphere, which further attenuates the radiance perceived by a sensor. Both of these effects are investigated below.

Kilauea Test Site

Plate 1a is a color-composite of TIMS data acquired over the Pu`u `O`o vent of Kilauea Volcano (Figure 3) on 30 September 1988. To create this composite image, data from TIMS Channels 5, 3, and 2 (see Figure 1) were displayed in red, green, and blue, respectively. In addition, these data were processed to depict temperature variations as changes in the brightness of the display colors (brighter colors signifying warmer temperatures) and spectral variations as changes in the hue and saturation of the display colors [cf. *Gillespie et al.,* 1986]. The absorption of ground radiance in Channel 2 causes the SO_2 plume to appear in hues of yellow and red in Plate 1a.

The Pu`u `O`o plume was assumed to be planar, with a thickness of 0.25 km. The altitude of the plume was 1.1 km, roughly 0.25 km above ground level, as determined from shadows cast by the plume [cf. *Realmuto et al.,* 1997]. The plume was imaged from an altitude of 1.9 km.

Profiles of atmospheric pressure, temperature, and relative humidity were obtained from a balloon-borne radiosonde launched by the National Weather Service from the Hilo Airport, which is located approximately 35 km north of Pu`u `O`o (cf. Figure 3). The radiosonde was launched four hours after the TIMS overflight.

Plate 1b is a map of the SO_2 column abundance derived from the TIMS data. This map shows that the distribution of SO_2 within the plume was not uniform. There were several high concentration cells, or puffs, entrained in a low-concentration stream. Detailed discussions of the SO_2 column abundance map and puffing behavior of Pu`u `O`o are available in *Realmuto et al.* [1997].

Plate 1c depicts the result of resampling the plume map to the spatial resolution of ASTER (Table 1). The non-uniform distribution of SO_2 within the plume is still recognizable, despite the dilution of the column abundance values. The column abundance estimates in the puffs range from 12 to 20 g m^{-2} and the column abundance in the low-concentration stream is typically less than 6 g m^{-2}.

Plate 1d depicts the result of resampling the plume map to the spatial resolution of MODIS (Table 1). At this resolution the Pu`u `O`o vent and plume are reduced to a single pixel (partial pixels resulting from the resampling process are not valid predictors of instrument response). The SO_2 column abundance estimate for this pixel is approximately 3 g m^{-2}.

The next step is to determine if ASTER and MODIS will have sufficient signal resolution, or sensitivity, to detect the SO_2 column abundance levels predicted by the resampling process. One measure of the sensitivity of a TIR instrument is the noise equivalent change in temperature, or NEΔT, which is the smallest change in temperature that can be detected in the presence of noise. The NEΔT specifications for the ASTER and MODIS TIR channels are found in Table 1.

Plate 1e contains simulations of the apparent reductions in ground temperature that would be perceived by a spaceborne instrument viewing the ground through the 1988 Pu`u `O`o plume. Hilo radiosonde data were used to describe the atmosphere up to 10 km and the MODTRAN tropical atmosphere model was used to describe the remainder of the path to space. An apparent change in ground temperature is the difference between the temperatures derived from radiance spectra calculated for a clear path and a path through an SO_2 plume.

The results of these simulations (Plate 1e) indicate that the apparent reduction in ground temperature resulting from SO_2 abundance levels of 10 and 15 g m^{-2} will exceed the 0.3 K NEΔT specified for the ASTER channels (Table 1). ASTER should be able to detect puffs similar to those in the 1988 Pu`u `O`o plume (Plate 1c), but lower abundance levels (5 g $m^{-2}$ or less) may not be detected. The low NE$\Delta$T of 0.05 K specified for the MODIS channels (Table 1) may allow the detection of Pu`u `O`o-scale plumes, but the detection of a single pixel many not be statistically significant.

Mount Etna Test Site

Plate 2a is a color composite of TIMS data acquired over Mount Etna (Figure 4) on 29 July 1986. This image was prepared in same manner as the Pu`u `O`o color composite (Plate 1a). The Etna plume was imaged from an altitude of 7.73 km.

The geometry of the Etna plume was described by a conical model. The altitude of the plume, or axis of the cone, was set at 3.5 km, slightly higher than the elevation of the crater complex at the summit of Etna (Figure 4). The thickness of the plume varied from 0.20 km near the summit, or the apex of the cone, to 0.50 km at the margin of the TIMS scene. This plume geometry is consistent with those measured during airborne surveys of the Etna plume [e.g. *Allard et al.,* 1991; *Jaeschke et al.,* 1982].

Profiles of atmospheric pressure, temperature, and relative humidity were obtained from a radiosonde launched from Trapani, which is located approximately 220 km west of Mount Etna (cf. Figure 4). The radiosonde launched approximately two hours prior to the TIMS overflight.

Plate 2b is the SO_2 column abundance map derived from the TIMS data. The highest levels of SO_2 are found near the source vents in the summit crater complex of Mount Etna (cf. Figure 4). The SO_2 abundance decreases with increasing distance from the vents due to dispersion and the scavenging of sulfur from the plume via the adsorption of sulfate aerosols onto ash particles [e.g. *Jaeschke et al.,* 1982, *Martin et al.,* 1986]. The distribution of SO_2 in the Etna plume does not display the high concentration cells, or puffs, that characterized the 1988 Pu`u `O`o plume (Plate 1b). There is little variation in SO_2 column abundance downwind of the source vent region.

A comparison of the TIMS (Plate 2b) and ASTER (Plate 2c) maps reveals that the basic structure of the Etna plume is recognizable at a spatial resolution of 90 m. Dilution is relatively minor in the downwind portion of the plume, due to the uniform SO_2 distribution and greater width of the plume. The highest dilution is found near the source vents, where the distribution of SO_2 was least uniform and the plume was narrow.

The basic structure of the Etna plume can also be recognized in the MODIS map (Plate 2d), but the source vent region is represented by a single pixel. The high level of dilution in this pixel, where a column abundance of 3.6 g m^{-2} replaces abundance levels in excess of 15 g m^{-2} (Plate 2b), is evidence that the source vents occupy a small fraction of a MODIS pixel. The width of the downwind portion of the plume, together with the uniformity of the SO_2 distribution, was sufficient to minimize dilution at the spatial resolution of MODIS.

To simulate the apparent reduction in ground temperatures (Plate 2e), Trapani radiosonde data were used to describe the atmosphere up to 10 km and the MODTRAN mid-latitude summer atmosphere model was used to describe the remainder of the path to space. A column abundance of 0.5 g m^{-2}, the cut-off value for the plume maps (Plates 2b, c, and d), resulted in an apparent

temperature change in excess of 0.60 K. Therefore, both ASTER and MODIS (Table 1) should be able to detect Mount Etna-scale plumes with little difficulty.

Discussion

Detection Limits. A comparison of Plates 1e and 2e underscores the importance of temperature contrast in the retrieval of SO_2. The temperature of the Etna and Pu`u `O`o plumes were 284 and 292 K, respectively (according to their respective radiosonde profiles). For the Etna simulations a ground temperature of 310 K (selected from the Etna ground temperature map for a ground target at an elevation of 3 km) was used, resulting in a temperature contrast of 26 K. For the Pu`u `O`o simulations a ground temperature of 304 K (selected from the Pu`u `O`o temperature map for a ground target at 0.85 km elevation) was used, resulting in a temperature contrast of 12 K. Consequently, the SO_2 detection limit derived from the Etna simulation is an order of magnitude lower than the limit derived from the Pu`u `O`o simulation.

Sources of Error. Potential sources of error in the retrieval procedure include incomplete knowledge of the plume geometry and local atmospheric conditions, use of a piecewise linear function to approximate the relationship between SO_2 column abundance and perceived radiance, and the calibration of the sensor. *Realmuto et al.* [1997] estimated that the error budget for TIMS-based SO_2 retrievals to be at least 20 %.

Sensitivity analyses [*Realmuto et al.,* 1994, 1997] indicate that plume altitude is the most important of the factors listed above, since the altitude defines the temperature contrast between the plume and background. There are several strategies for determining plume altitude in the absence of direct field observations. The simplest strategy is to assume that the plume altitude is approximately equal to the elevation of the source vent. This approach was used in the construction of the Mount Etna plume map (Plate 2a).

A more refined altitude-determination strategy is to use shadows cast by the plume, together with the solar azimuth and elevation at the time the image was acquired, to calculate the plume altitude [e.g. *Glaze et al.,* 1989; *Holasek and Self,* 1995; *Realmuto et al.,* 1997]. This approach was used in the construction of the Pu`u `O`o plume map (Plate 1a). *Glaze et al.* [1999] have developed an altitude-estimation technique based on photoclinometry, in which the brightness (reflectance) of an image pixel is converted to an estimate of the orientation of the surface represented by the pixel relative to the sun. The relative elevation of a surface element within a row or column of image data is determined from the cumulative slope along this row or column.

Stereo imagery can also be used to determine the altitude of plumes [e.g. *Prata and Turner,* 1997]. ASTER will have nadir and aft-viewing telescopes capable of acquiring stereo images with a ground resolution (at nadir) of 15 m. The ASTER Project plans to produce digital elevation models (DEM's) with 30 m spatial resolution and 7 to 50 m vertical accuracy [*Welch et al.,* 1998]. DEM's generated without the use of ground control points will have a relative accuracy of 10 – 30 m, which may be sufficient for volcanic plume mapping. Individual scientists will be able to generate ASTER DEM's with commercial, off-the-shelf software.

The lack of local radiosonde data to determine atmospheric profiles can be partially offset by the use of MODTRAN climatology profiles. However, the MODTRAN profiles provide little spatial or temporal resolution. The use of global climate assimilation models can provide spatial resolution on the order of 2 degrees (of longitude and latitude) and temporal resolution on the order of 3 to 6 hours [*Schubert et al.,* 1993].

Meteorological clouds at sub-pixel resolutions are an additional source of error in ASTER and MODIS SO_2 retrievals. Plate 2a shows a train of opaque clouds, which may have been

formed of water droplets that condensed from the Etna plume. These clouds were omitted from the TIMS plume map (Plate 2b) and, due to the high spatial resolution of ASTER, the clouds were largely omitted from the ASTER map (Plate 2c). The MODIS map (Plate 2d) incorporates these clouds, since they are too small to be resolved in the MODIS data. Imagery from the ASTER and MODIS visible and near infrared channels, which will have higher spatial resolution than the corresponding TIR channels, could be used to delineate cloud-contaminated pixels prior to SO_2 retrieval. Cloud masks such as these will be standard products of the ASTER and MODIS science teams [*Justice et al.*, 1998; *Logar et al.,* 1998].

Application to Products of Explosive Eruptions

The explosive injection of volcanic material into the atmosphere has important implications for climate forcing [e.g. *Lacis et al.,* 1992; *McCormick et al.,* 1995] and aircraft safety [e.g. *Dunn and Wade,* 1994; *Casadevall and Krohn,* 1995]. The potential application of TIR SO_2 retrieval to eruption columns and volcanic clouds is discussed in this section.

Eruption Columns

The properties of eruption columns will likely prevent the accurate retrieval of SO_2 using the techniques discussed in this paper. Eruption columns are typically opaque to TIR radiation [cf. *Holasek and Self,* 1995; *Holasek et al.,* 1996]. Due to this opacity, ground radiance is not transmitted through the column and any SO_2 absorption features are saturated. The top of a column may not be in thermodynamic equilibrium with the surrounding atmosphere, so the estimation of column altitude from column temperature can be problematic [*Woods and Self,*

1992; *Holasek and Self,* 1995; *Holasek et al.,* 1996]. Finally, the columns are typically not isothermal [*Sparks et al.,* 1997], invalidating the plane-parallel atmosphere model incorporated in MODTRAN.

Volcanic Clouds

The application of TIR SO_2 retrievals to volcanic clouds is in many ways analogous to the TIR detection of ash and aerosols in such clouds [e.g., *Prata,* 1989a and b; *Wen and Rose,* 1994]. The successful detection of ash clouds from a variety of recent eruptions [e.g., *Prata,* 1989a and b; *Holasek and Rose,* 1991; *Wen and Rose,* 1994; *Schneider et al.,* 1995] lends optimism to the application of TIR SO_2 retrievals to SO_2 clouds.

SO_2 clouds will present at least one obstacle to the application of the retrieval techniques discussed in this paper. The clouds typically contain mixtures of SO_2, sulfate aerosols, silicate ash, and ice - materials that exhibit absorption and emission in the 10 – 12 μm spectral region [e.g., *Prata* 1989a, *Wen and Rose,* 1994], currently used as a "clear path" to estimate the temperature of the ground beneath a plume. Therefore, it will be difficult to accommodate any changes in ground temperature beneath the cloud.

This obstacle will be partially mitigated by the high probability that an SO_2 cloud will lie over a body of water. In this scenario the background temperature can be estimated from "clear" pixels found adjacent to the cloud [e.g., *Wen and Rose,* 1994].

Figure 5 is a simulation of the apparent reduction in ground temperature perceived by a spaceborne sensor viewing the ground through an SO_2 cloud. The cloud properties are taken from the 19 August 1992 eruption of Mount Spurr (Alaska). TOMS observations of the SO_2

clouds yielded column abundance estimates of 1.43 g m^{-2} [*Bluth et al.,* 1995]. National Weather Service radar measurements determined that the maximum altitude of the eruption column was 13.5 km [*Rose et al.,* 1995]. *Wen and Rose* [1994] reported a sea surface temperature of 273 K in their study of Mount Spurr ash clouds over the Pacific Ocean. The simulation produced an apparent change in ground temperature in excess of 3.5 K (Figure 5), suggesting that both ASTER and MODIS will detect such SO_2 clouds with little difficulty.

Conclusions

The objective of this research was to determine if passive SO_2 emissions could be detected at the spatial and signal resolutions specified for ASTER and MODIS. Both ASTER and MODIS should detect emissions on the scale (SO_2 concentration and plume geometry) of the 1986 Mount Etna SO_2 plume. ASTER should detect emissions on the scale of the 1988 Pu`u `O`o plume. MODIS may also detect Pu`u `O`o-scale plumes, but the results may not be statistically significant. In addition, both ASTER and MODIS should detect SO_2 clouds on the scale of those produced by the 1992 eruption of Mount Spurr.

Thus ASTER and MODIS will be important new tools for volcano monitoring and studies of volcanic plumes and clouds. The data from these instruments could be used to establish baseline emission rates for various volcanoes around the world, detect deviations from the baseline rates, and map the atmospheric products of explosive eruptions. SO_2 retrievals from ASTER and MODIS data could be used to validate TOMS SO_2 retrievals.

The combined use of ASTER, MODIS, and TOMS could allow volcanologists and atmospheric scientists to document the life cycle of volcanogenic sulfur in the atmosphere. In

the initial phases of an eruption, when the eruption column is opaque, TOMS will be the principal source of SO_2 information. As SO_2 clouds form and become transparent to TIR radiation, all three instruments will detect them. This phase of observation will also provide data for the cross-validation of the UV and TIR retrieval techniques. As the SO_2 clouds become too depleted to be detected by TOMS, the higher spatial resolution of ASTER and MODIS will allow the detection to continue. ASTER will be the last instrument to detect the clouds as the depletion of SO_2 continues. Finally, the recent use of radiance measurements in the 8 – 12 μm region to detect volcanogenic H_2SO_4 aerosols [*Baran et al.,* 1993; *Ackerman and Strabala,* 1994] hint that ASTER and MODIS data might be applied to studies of the conversion of SO_2 to sulfate aerosols.

Acknowledgments

The author thanks J. Crisp, S. Williams, and K. Dean for their through reviews of this manuscript. Support for this research was provided by NASA's Solid Earth and Natural Hazards and EOS Interdisciplinary Study programs. The author is a member of the EOS Volcanology IDS Team, which is led by P. Mouginis-Mark of the University of Hawaii at Manoa. This research was conducted at the Jet Propulsion Laboratory, California Institute of Technology, under contract to the National Aeronautics and Space Administration.

References

Ackerman, S. A., and K. I. Strabala, Satellite remote sensing of H_2SO_4 aerosol using the 8- to 12 μm window region: application to Mount Pinatubo, *J. Geophys. Res., 99,* 18,639-18,649, 1994.

Allard, P., J. Carbonnelle, D. Dajlevic, J. Le Bronec, P. Morel, M. C. Robe, J.M. Maurenas, R. Faivre-Pierret, D. Martin, J. C. Sabroux, and P. Zettwoog, Eruptive and diffuse emissions of CO_2 from Mount Etna, *Nature, 351,* 387-391, 1991.

Andres, R. J., W. I. Rose, P. R. Kyle, S. deSilva, P. Francis, M. Gardeweg, and H. Moreno-Roa, Excessive sulfur dioxide emissions from Chilean volcanoes, *J. Volcanol. Geotherm. Res., 46,* 323-329, 1991.

Baran, A. J., J.S. Foot, and P.C. Dibben, Satellite detection of volcano sulphuric acid aerosol, *Geophys. Res. Lett., 20,* 1799-1801, 1993.

Barnes, W. L., T. S. Pagano, and V. V. Salomonson, Prelaunch characteristics of the moderate resolution imaging spectrometer (MODIS) on EOS-AM1, *IEEE Trans. Geosci. Remote Sens., 36,* 1088 – 1100, 1998.

Berresheim, H., and W. Jaeschke, The contribution of volcanoes to the global atmospheric sulfur budget, *J. Geophys. Res., 88,* 3732-3740, 1983.

Berk, A; L.S. Bernstein, and D. C. Robertson, MODTRAN: a medium resolution model LOWTRAN-7, *GL-TR-89-0122,* 1989.

Bluth, G. J. S., S. D. Doiron, C. C. Schnetzler, A. J. Krueger, and L. S. Walter, Global tracking of the SO_2 clouds from the June 1991 Mount Pinatubo Eruptions, *Geophys. Res. Lett., 19,* 151-154, 1992.

Bluth, G. J. S., C. C. Schnetzler, A. J. Krueger, and L. S. Walter, The contribution of explosive volcanism to global atmospheric sulphur dioxide concentrations, *Nature, 336,* 327-329, 1993.

Bluth, G. J. S., T. J. Casadevall, C. C. Schnetzler, S. D. Doiron, L. S. Walter, A. J. Kreuger, and M. Badruddin, Evaluation of sulfur dioxide emissions from explosive volcanism: the 1982-1983 eruptions of Galunggung, Java, Indonesia, *J. Volcanol. Geotherm. Res., 63,* 243-256, 1994.

Bluth G. J. S., C. J. Scott, I. E. Sprod, C. C. Schnetzler, A. J. Krueger, and L. S. Walter, Explosive emissions of sulfur dioxide from the 1992 Crater Peak eruptions, Mount Spurr, Alaska, *USGS Bull. 2139,* 47-57, 1995.

Bluth G. J. S, W.I. Rose, I.E. Sprod, and A. J. Krueger, Stratospheric loading of sulfur from explosive volcanic eruptions, *J. Geology, 105,* 671-683, 1997.

Caltabiano, T., R. Romano, and G. Budetta, SO_2 flux measurements at Mount Etna (Sicily). *J. Geophys. Res., 99,* 12,809-12,819, 1994.

Casadevall, T. J., D. A. Johnston, D. M. Harris, W. I. Rose, L. L. Malinconico, R. E. Stoiber, T. J. Bornhorst, S. N. Williams, L. Woodruff, and J. M. Thompson, SO_2 Emission Rates at Mount St. Helens from March 29 through December 1980, in *USGS Prof. Paper 1250,* 193-200, 1981.

Casadevall, T. J., W. I. Rose, T. Gerlach, L. P. Greenland, J. Ewert, R. Wunderman, and R. Symonds, Gas emissions and the eruptions of Mount St. Helens through 1982, *Science, 221,* 1383-1385, 1983.

Casadevall, T. J., A. J. Krueger, and J. B. Stokes, The volcanic plume from the 1984 eruption of Mauna Loa, Hawaii, *EOS Trans. AGU, 65,* 1133, 1984.

Casadevall, T. J., J. B. Stokes, L. P. Greenwood, L. L. Malinconico, J. R. Casadevall, and B. T. Furukawa, SO_2 and CO_2 emission rates at Kilauea Volcano, 1979-1984, in *USGS Prof. Paper 1350,* edited by R. Decker, T. Wright, and P. Stauffer, pp. 771-780, 1987.

Casadevall, T. J. , and M. D. Krohn, Effects of the 1992 Crater Peak eruptions on airports and aviation operations in the United States and Canada, *USGS Bull. 2139,* 1995.

Chartier, T. A., W. I. Rose, and J. B. Stokes, Detailed record of SO_2 emissions from Puu Oo between episodes 33 and 34 of the 1983-1986 ERZ eruption, Kilauea, Hawaii, *Bull. Volcanol., 50,* 215-228, 1988.

Daag, A. S., B. S. Tubianosa, C. G. Newhall, N. M. Tungol, D. Javier, M. T. Dolan, P. J.Delos Reyes, R. A. Arboleda, M. L. Martinez, and T. M. Regalado, Monitoring sulfur dioxide emission at Mount Pinatubo, in *Fire and Mud: Eruptions and Lahars of Mount Pinatubo, Philippines,* edited by C. G. Newhall and R.S. Punongbayan, pp. 409-414, University of Washington Press, Seattle, 1996.

Doiron, S. D., G. J. S. Bluth, C. C. Schnetzler, A. J. Krueger, and L. S. Walter, Transport of Cerro Hudson SO_2 clouds, *EOS Trans. AGU, 72,* 489-498, 1991.

Dunn, M. G., and D. G. Wade, Influence of volcanic ash clouds on gas turbine engines, *USGS Bull. 2047*, 107-118, 1994.

Elias T., A. J. Sutton, and J. B. Stokes, Current SO_2 emissions at Kilauea Volcano: quantifying scattered degassing sources, *EOS Trans. AGU, 74,* 670-671, 1993.

Gillespie, A. R., A. B. Kahle, and R. E. Walker, Color enhancement of highly correlated images. I. decorrelation and HSI contrast stretches, *Remote Sens. Environ., 20,* 209-235, 1986.

Glaze, L. S., P. W. Francis, S. Self, and D. A. Rothery, The 16 September 1986 eruption of Lascar Volcano, noth Chile: satellite investigations. *Bull. Volcanol., 51, 149-160,* 1989.

Glaze, L. S., L. Wilson, and P. J. Mouginis-Mark, Volcanic eruption plume top topography and heights as determined from photoclinometric analysis of satellite data, *J. Geophys. Res. 104,* 2989-3001, 1999.

Graf, H.-F., J. Feichter, and B. Langmann, Volcanic sulfur emissions: estimates of source strength and its contribution to the global sulfate distribution, *J. Geophys. Res., 102,* 10,727-10,738, 1997.

Holasek R. E., and W. I. Rose, Anatomy of the 1986 Augustine volcano eruptions as recorded by multispectral image processing of digital AVHRR weather satellite data, *Bull. Volcanol., 53,* 420-435, 1991.

Holasek, R. E., and S. Self, GOES weather satellite observations and measurements of the May 18, 1980, Mount St. Helens eruption, *J. Geophys. Res., 100,* 8469-8487, 1995.

Holasek, R. E., S. Self, and A. W. Woods, Satellite observations and interpretations of the 1991 Mount Pinatubo eruption plumes, *J. Geophys. Res., 101,* 27,635-27,655, 1996.

Jaeschke, W., H. Berresheim, and H.-W. Georgii, Sulfur emissions from Mt. Etna, *J. Geophys. Res., 87,* 7253-7261, 1982.

Justice, C. O., E. Vermote, J. R. G. Townshend, D. P. Roy, D. K. Hall, V. V. Salomonson, J. L. Privette, G. Riggs, A. Strahler, W. Lucht, R. B. Myneni, Y. Knyazikhin, S. W. Running,

R. R Nemani, Z. Wan, A. R. Huete, W. van Leeuwen, R. E. Wolfe, L. Giglio, J.-P. Mueller, P. Lewis, and M. J. Barnsley, The moderate resolution imaging spectroradiometer (MODIS): land remote sensing for global change research, *IEEE Trans. Geosci. Remote Sens., 36,* 1228-1249, 1998.

Kahle, A. B., F. D. Palluconi, S. J. Hook, V. J. Realmuto, and G. Bothwell, The Advanced Spaceborne Thermal Emission and Reflectance Radiometer (ASTER), *Int. J. Imaging Sys. Tech., 3,* 144-156, 1991.

Krueger, A. J., Sighting of El Chichón sulfur dioxide clouds with the Nimbus 7 Total Ozone Mapping Spectrometer, *Science, 220,* 1377-1379, 1983.

Krueger, A. J., L. S. Walter, C. C. Schnetzler, and S. D. Doiron, TOMS measurement of the sulfur dioxide emitted during the 1985 Nevado del Ruiz eruptions, *J. Volcanol. Geotherm. Res., 41,* 7-15, 1990.

Krueger A. J., L. S. Walter, P. K. Bhartia, C. C. Schnetzler, N. A. Krotkov, I. Sprod, and G. J. S. Bluth, Volcanic sulfur dioxide measurements from the Total Ozone Mapping Spectrometer (TOMS) instruments, *J. Geophys. Res., 100,* 14,057-14,076, 1995.

Kyle, P. R., K. Meeker, and D. Finnegan, Emission rates of sulfur dioxide, trace gases, and metals from Mount Erebus, Antarctic, *Geophys. Res. Lett., 17,* 2125-2128, 1990.

Kyle, P. R., L. M. Sybeldon, W. C. McIntosh, K. Meeker, and R. Symonds, Sulfur dioxide emission rates from Mount Erebus, Antarctica, in *Antarctic Research Series, Vol. 66, Volcanological and Environmental Studies of Mount Erebus, Antarctica,* edited by P.R. Kyle, pp. 69-82, 1994.

Lacis, A., J. Hansen, and M. Sato, Climate forcing by stratospheric aerosols, *Geophys. Res. Lett.,* 19, 1607-1610, 1992.

Logar, A. M., D. E. Lloyd, E. M. Corwin, M.L. Penaloza, R. E. Feind, T. A. Berendes, K.-S. Kuo, and R. M. Welch, The ASTER polar cloud mask, *IEEE Trans. Geosci. Remote Sens., 36,* 1302-1312, 1998.

Martin, D., B. Ardouin, G. Bergametti, J. Carbonelle, R. Faivre-Pierret, G. Lambert, M. F. Le Cloarec, and G. Sennequier, Geochemistry of sulfur in Mount Etna plume, *J. Geophys. Res., 91,* 12,249-12,254, 1986.

McCormick M.P., L.W. Thomason, and C. R. Trepte, Atmospheric effects of the Mt. Pinatubo eruption, *Nature, 373,* 399-404, 1995.

McGee, K. A., The structure, dynamics, and chemical composition of noneruptive plumes from Mount St. Helens, 1980-88, *J. Volcanol. Geotherm. Res.,* 51, 269-282, 1992.

McGee, K. A., and A. J. Sutton, Eruptive activity at Mount St. Helens, Washington, USA, 1984-1988: a gas geochemistry perspective, *Bull. Volcanol., 56,* 433-446, 1994.

Moffat, A. J., and M. M. Millán, The applications of optical correlation techniques to the remote sensing of SO_2 plumes using sky light, *Atmos. Environ., 5,* 677-690, 1971.

Newcomb, G. S., and M. M. Millán, Theory, applications, and results of the long-line correlation spectrometer, *IEEE Trans. Geosci. Electron., GE 8,* 149-157, 1970.

Prata, A. J., Infrared radiative transfer calculations for volcanic ash clouds, *Geophys. Res. Lett., 16,* 1293-1296, 1989a.

Prata, A. J., Observations of volcanic ash clouds in the 10 – 12 μm window using AVHRR/2 data, *Int. J. Remote Sens., 10,* 751-761, 1989b.

Prata, A. J., and P. J. Turner, Cloud-top height determination using ATSR data, *Remote Sens. Environ., 59,* 1-13, 1997.

Pyle, D. M., P. D. Beattie, and G. J. S. Bluth, Sulphur emissions to the stratosphere from explosive volcanic eruptions, *Bull. Volcanol., 57,* 663-671, 1996.

Realmuto, V. J., M. J. Abrams, M. F. Buongiornio, and D.C. Pieri, The use of multispectral thermal infrared image data to estimate the sulfur dioxide flux from volcanoes: a case study from Mount Etna, Sicily, July 29, 1986, *J. Geophys. Res., 99,* 481-488, 1994.

Realmuto, V. J., A. J. Sutton, and T. Elias, Multispectral thermal infrared mapping of sulfur dioxide plumes: a case study from the East Rift Zone of Kilauea Volcano, Hawaii, *J. Geophys. Res. 102,* 15,057-15,072, 1997.

Rose, W. I., R. L. Chuan, W. F. Giggenbach, P. R. Kyle, and R. B. Symonds, Rates of sulfur dioxide and particle emissions from White Island volcano, New Zealand, and an estimate of the total flux of major gaseous species, *Bull. Volcanol., 48,* 181-188, 1986.

Rose, W. I., G. Heiken, K. Wohletz, D. Eppler, S. Barr, T. Miller, R. L. Chuan, and R. B. Symonds, Direct rate measurements of eruption plumes at Augustine volcano: a problem of scaling and uncontrolled variables, *J. Geophys. Res., 93,* 4485-4499, 1988.

Rose, W. I., A. B. Kostinski, and L. Kelley, Real-time C-band radar observations of the 1992 eruption clouds from Crater Peak, Mount Spurr Volcano, Alaska, *USGS Bull. 2139,* 19-26, 1995.

Schneider, D. J., W. I. Rose, and L. Kelley, Tracking of 1992 eruption clouds from Crater Peak Vent of Mount Spurr Volcano, Alaska, using AVHRR, *USGS Bull. 2139,* 27-36, 1995.

Schubert, S. D., R. B. Rood, and J. Pfaendtner, An assimilated dataset for earth-science applications, *Bull. Am. Meteorol. Soc., 74,* 2331-2342, 1993.

Stephens, G. L., *Remote Sensing of the Lower Atmosphere,* 523 pp., Oxford University Press, New York, 1994.

Stoiber, R. E., S. N. Williams, and B. Huebert, Annual contribution of sulfur dioxide to the atmosphere by volcanoes, *J. Volcanol. Geotherm. Res., 33,* 1-8, 1987.

Sparks, R. S. J., M. I. Bursik, S. N. Carey, J. S. Gilbert, L. S. Glaze, H. Sigurdsson, and A. W. Woods, *Volcanic Plumes,* 574 pp., John Wiley and Sons, New York, 1997.

Walter, L. S., G. J. S. Bluth, C. C. Schnetzler, I. E. Sprod, and A. J. Krueger, Satellite observations of SO_2 emissions from the 1984 Mauna Loa eruption. *EOS Trans. AGU 74,* 636, 1993.

Welch, R., T. Jordan, H. Lang, and H. Murakami, ASTER as a source of topographic data in the late 1990's, *IEEE Trans. Geosci. Remote Sens., 36,* 1282-1289, 1998.

Wen, S., and W. I. Rose, Retrieval of sizes and total masses of particles in volcanic clouds using AVHRR bands 4 and 5, *J. Geophys. Res.,* 99, 5421-5431, 1994.

Williams, S. N., N. C. Sturchio, M.L. Calvache, R. Mendez, A. Londoño, and N. García, Sulfur dioxide from Nevado del Ruiz volcano, Colombia: total flux and isotopic constraints on its origin. *J. Volcanol. Geotherm. Res., 42*, 53-68, 1990.

Woods, A. W. and S. Self, Thermal disequilibrium at the top of volcanic clouds and its effects on estimates of the column height, *Nature, 355,* 628-630, 1992.

Yamaguchi Y, A. B. Kahle, H. Tsu, T. Kawakami, and M. Pniel, Overview of advanced spaceborne thermal emission and reflection radiometer (ASTER), *IEEE Trans. Geosci. Remote Sens.*, 36, 1062-1071, 1998.

Zapata, J.A., M. L. Calvache, G.P. Cortes, T.P. Fischer, G. Garzon, D. Gomez, L. Narvaez, M. Ordoñez, A. Ortega, J. Stix, R. Torres, and S.N. Williams, SO_2 fluxes from Galeras Volcano, Colombia, 1989-1995: progressive degassing and conduit obstruction of a Decade Volcano. *J. Volcanol. Geotherm. Res. 77,* 195-208, 1997.

Zreda-Gostynska G., and P. R. Kyle, Chlorine, fluorine, and sulfur emissions from Mount Etna, Antarctica, and estimated contributions to the antarctic atmosphere. *Geophys. Res. Lett. 20,* 1959-1962, 1993.

Captions

Figure 1. Change in atmospheric transmission resulting from the introduction of an SO_2 plume. The heavy line represents the ratio of transmission through an atmospheric column containing 0.1 g m^{-2} of SO_2 to that of a column containing no SO_2 . The transmission ratio is superimposed on the normalized spectral response functions of the six TIMS channels, which are depicted as shaded regions.

Figure 2. Misfit surface, depicting the least squares misfit between a radiance spectrum calculated with a ground temperature of 305 K and SO_2 concentration of 10 mg m^{-3} with spectra generated for temperatures ranging from 295 to 315 K and concentrations ranging between 0 and 20 mg m^{-3}. Also shown are the profiles across the misfit surface in the temperature and concentration dimensions.

Figure 3. Location of the Pu`u `O`o vent of Kilauea Volcano relative to the summits of Kilauea and Mauna Loa and the city of Hilo.

Figure 4. Simplified topographic map of the summit of Mount Etna, showing the locations of craters in the summit crater complex. The inset shows the location of Mount Etna with respect to the Island of Sicily and Italian peninsula.

Figure 5. Simulation of the apparent change in ground temperature perceived by a spaceborne sensor viewing the ground through a volcanic cloud generated by the 19 August 1992 eruption of Mount Spurr.

Plate 1. Comparison of Pu`u `O`o plume maps at the spatial resolutions of TIMS (b), ASTER (c), and MODIS (d). Included are a color composite of the TIMS data (a), and the results of simulations of the apparent changes in ground temperature perceived by a spaceborne sensor viewing the ground through the 30 September 1988 Pu`u O`o plume (e).

Plate 2. Comparison of Mount Etna plume maps at the spatial resolutions of TIMS (b), ASTER (c), and MODIS (d). Included are a color composite of the TIMS data (a), and the results of simulations of the apparent changes in ground temperature perceived by a spaceborne sensor viewing the ground through the 29 July 1986 Etna plume (e).

Table 1. Characteristics of ASTER and MODIS, as specified by the respective science teams. Data obtained from *Kahle et al.,* [1991], *Barnes et al.,* [1998], and *Yamaguchi et al.,* [1998].

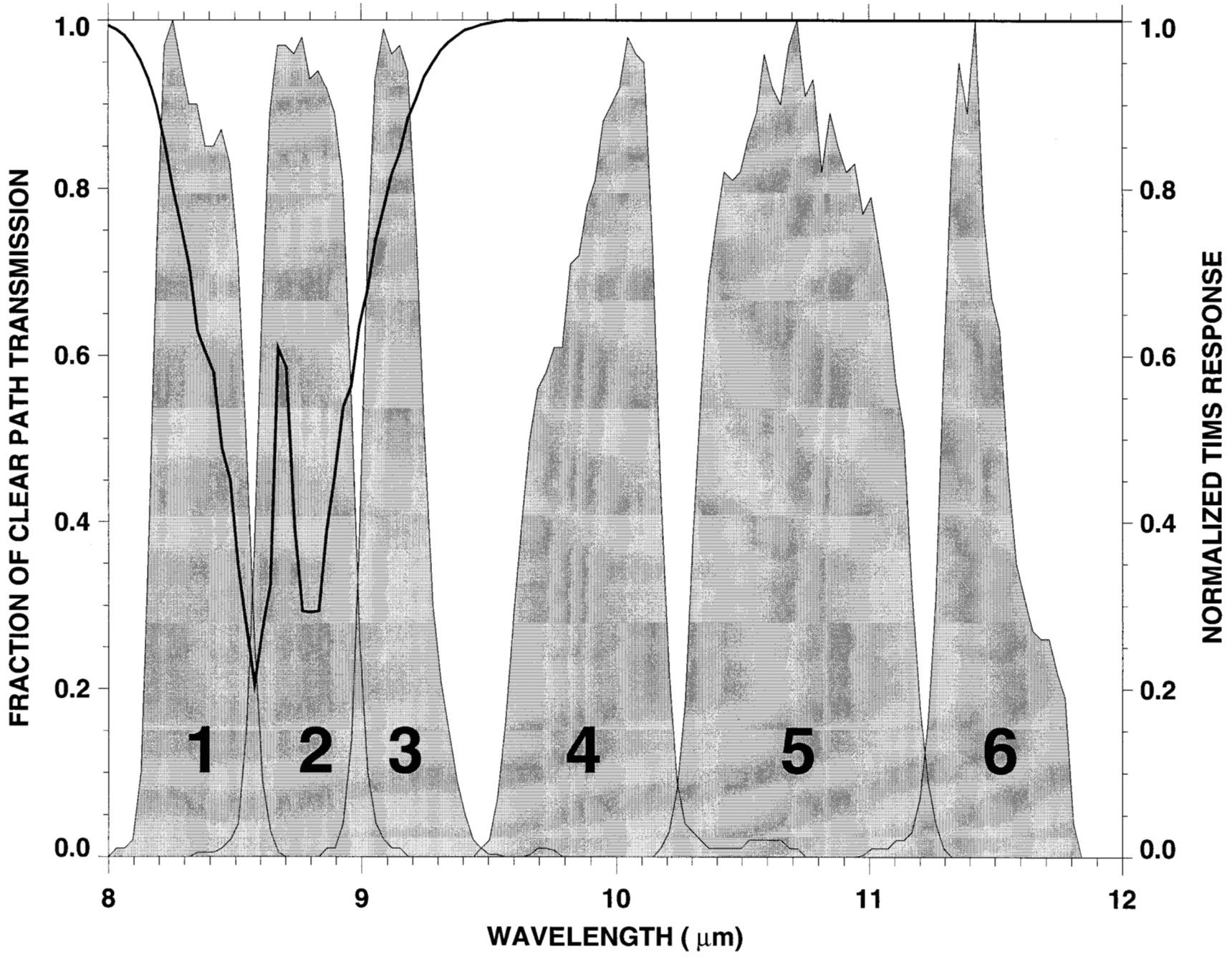
FRACTION OF CLEAR PATH TRANSMISSION
NORMALIZED TIMS RESPONSE
WAVELENGTH (μm)
1.0
0.8
0.6
0.4
0.2
0.0
8
9
10
11
12
1
2
3
4
5
6

Fig. 1

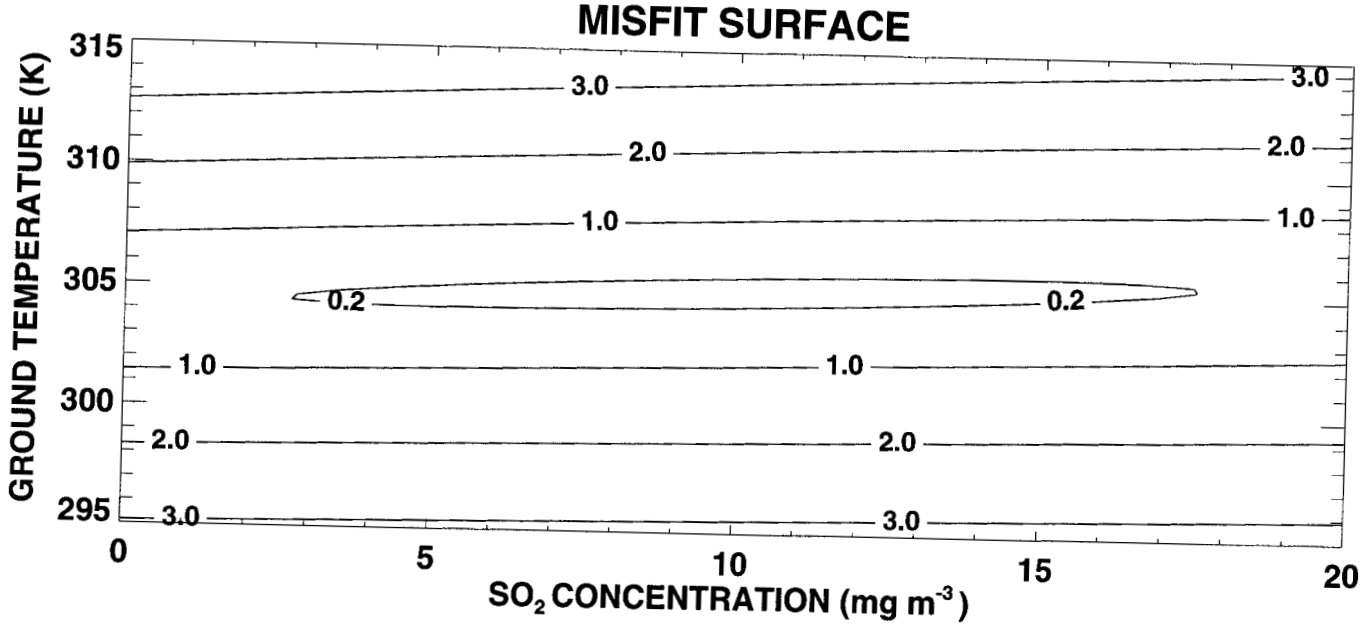
MISFIT SURFACE
GROUND TEMPERATURE (K)
315
310
305
300
295
3.0
2.0
1.0
0.2
0
5
10
15
20
SO2 CONCENTRATION (mg m-3)

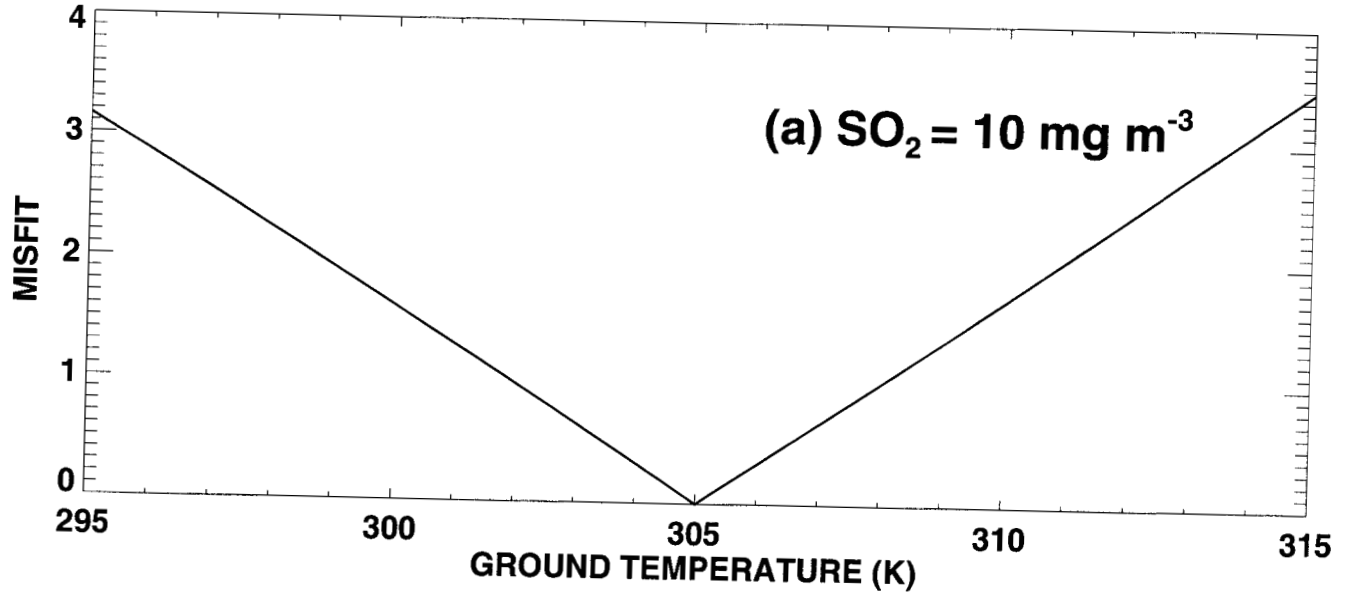
(a) SO2 = 10 mg m-3
MISFIT
4
3
2
1
0
295
300
305
310
315
GROUND TEMPERATURE (K)

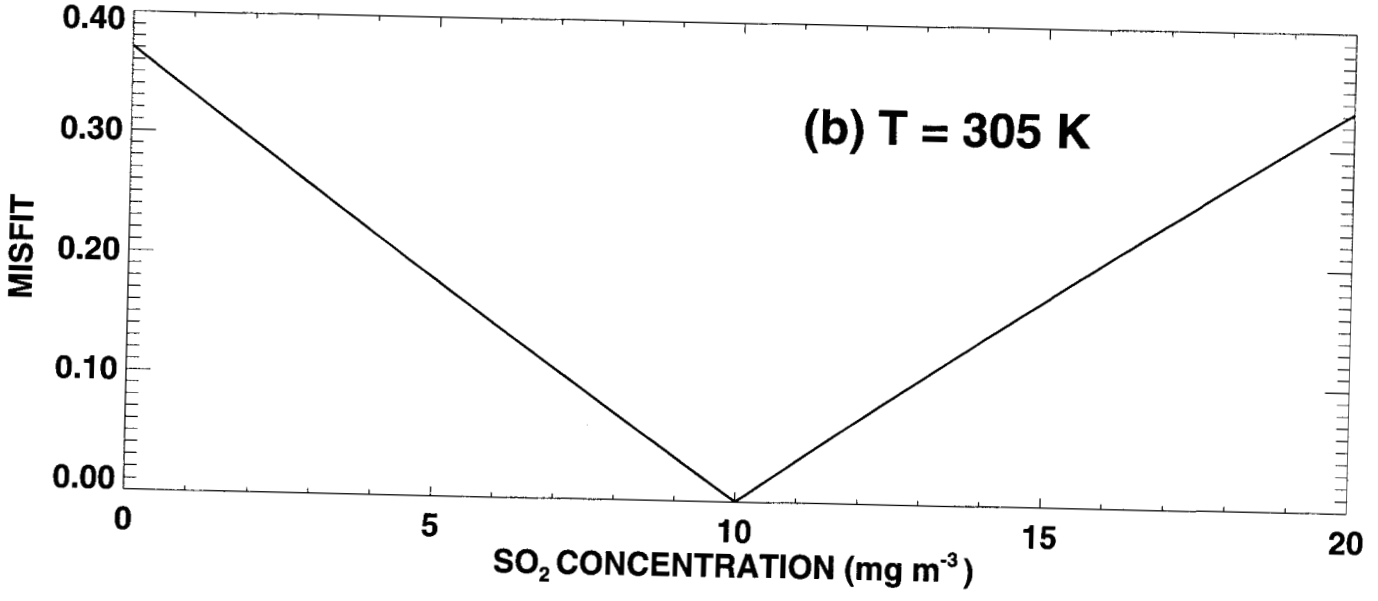
(b) T = 305 K
MISFIT
0.40
0.30
0.20
0.10
0.00
0
5
10
15
20
SO2 CONCENTRATION (mg m-3)

Fig. 2

hawaii_site_map.psd (4040x5560x256 psd)

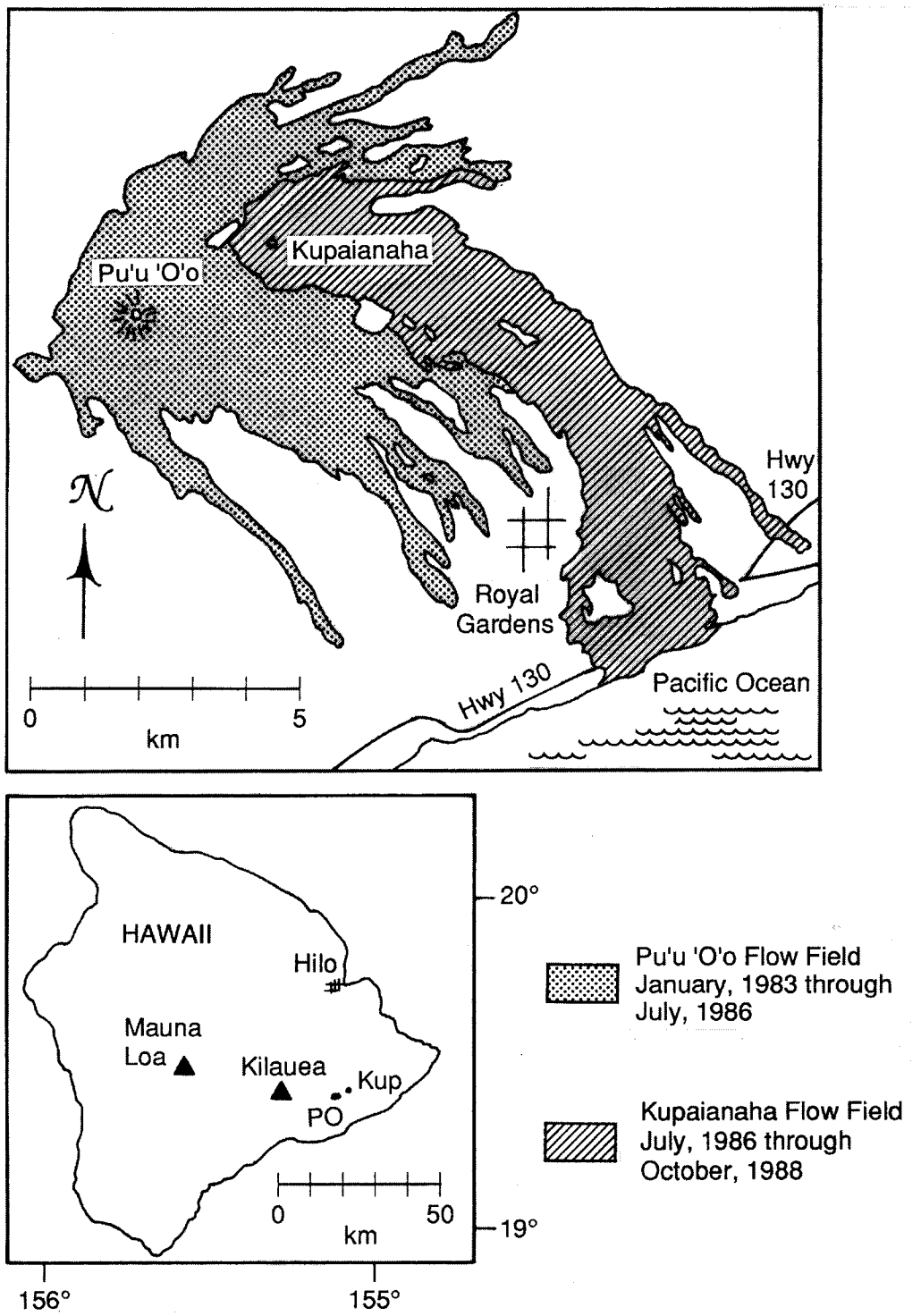

Figure 3